Optical Materials 145 (2023) 114371

Contents lists available at ScienceDirect

Optical Materials

journal homepage: www.elsevier.com/locate/optmat

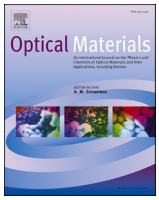

Research Article

Comparison of Al/TiO_2/p-Si and Al/ZnO/p-Si photodetectors

D. Esra Yıldız [a,**], Adem Kocyigit [b,*], Murat Yıldırım [c]

[a] Department of Physics, Faculty of Arts and Sciences, Hitit University, 19030, Corum, Turkey
[b] Department of Electronics and Automation, Vocational High School, Bilecik Şeyh Edebali University, 11000, Bilecik, Turkey
[c] Department of Biotechnology, Faculty of Science, Selcuk University, 42130, Konya, Turkey

ARTICLE INFO

Keywords:
TiO_2
ZnO
ALD
Photodetectors
Responsivity

ABSTRACT

The importance of the photodetectors has grown due to their potential in the automation system and optical communications. We fabricated Al/TiO_2/p-Si and Al/ZnO/p-Si Schottky-type photodetectors. TiO_2 and ZnO interlayers were grown by atomic layer deposition (ALD). The photodetection properties of these devices were studied and compared by *I–V* and *I-t* measurements for various light power densities and various wavelengths. Scanning electron microscopy (SEM) and energy dispersive X-ray (EDX) spectra were employed to determine morphological and elemental analysis of the TiO_2 and ZnO interlayers. While the SEM images showed smooth surfaces, EDX spectra approved successful synthesis of the TiO_2 and ZnO interlayers with good stoichiometry. The diode parameters such as ideality factor, series resistance and barrier height values were calculated and compared in detail. The responsivity and detectivity of the fabricated photodetectors were determined as a function of illumination power density and wavelength. The responsivity values of the Al/TiO_2/p-Si and Al/ZnO/p-Si photodetectors were determined as 0.02 and 0.76 A/W, respectively. Both photodetectors exhibited good performance for visible light. However, Al/ZnO/p-Si photodetector reached 173.08% external quantum efficiency (EQE) for 550 nm. According to results, Al/ZnO/p-Si photodetector exhibited better detection performance than Al/TiO_2/p-Si.

1. Introduction

Nowadays, fast growing technology of automation and wireless communication needs very sensitive detectors with better performance [1–4]. Among the detectors, photodetectors are used to detection of light for various wavelengths of optical region in the electromagnetic spectrum [5]. Various materials, designs and techniques have been studied to improve performance of the photodetection [6–9]. TiO_2 and ZnO are generally used for detection of light in the UV region. Gao et al., synthesized TiO_2 nanorods by hydrothermal method, and used them with p-type NiO flakes layer to obtain high performance UV photodetection on FTO glass [10]. Nicolaescu et al., obtained n-TiO_2/p--$CuMnO_2$ thin film by thermal oxidation of n-TiO_2 and doctor blade technique for p-$CuMnO_2$ to fabricate heterostructure p-n type photodetector for high responsivity performance [11]. Inamdar et al., fabricated metal-semiconductor-metal (MSM) based ZnO photodetectors by spray pyrolysis technique, and obtained photodetector exhibiting good performance at the UV-A region [12]. Liu et al., fabricated ZnO nanowires/Te nanowires heterojunction photodetector by two-step vacuum filtration, and they achieved high responsivity and detectivity values of~10 A/W and~10^{14} Jones for UV light detection, respectively. Sometimes, TiO_2 and ZnO are used as interfacial layer for Schottky-type photodetector to obtain good photodetection property for sun light [13–15]. If the TiO_2 and ZnO are deposited on the Si substrate to obtain photodetector, the device exhibits good performance in UV and visible regions [16,17].

There are many techniques to fabricate interlayers of thin films such as spin coating [18], chemical bath deposition [19], spray pyrolysis [20], electrodeposition [21], atomic layer deposition (ALD) [13] etc. Among them, ALD technique has many advantages such as large area uniformity, precise thickness control, high film density, repeatability, low temperature process and good stoichiometric control [22]. The ALD technique can produce suitable interlayers for the Schottky-type photodetectors.

Schottky-type photodetectors are metal-semiconductor junctions, fabricated generally by physical vapor deposition techniques [23,24,53]. The p-type or n-type Si is generally preferred to obtain these type of photodetectors, and a metal oxide or polymer layers sometimes are

* Corresponding author.
** Corresponding author.
E-mail addresses: desrayildiz@hitit.edu.tr (D.E. Yıldız), adem.kocyigit@bilecik.edu.tr (A. Kocyigit).

https://doi.org/10.1016/j.optmat.2023.114371
Received 11 May 2023; Received in revised form 11 August 2023; Accepted 13 September 2023
Available online 21 September 2023

inserted between the semiconductor and metal to control the current conduction mechanism and to passivate dangling bonds [25]. Both the TiO_2 and ZnO have high dielectric constants (over 23 and 8.0, respectively) and wide band gaps, 3.1 eV for TiO_2 and 3.4 for ZnO [26,27]. Thus, both the TiO_2 and ZnO can be used in the Schottky-type photodetector for visible light detection. Aim of this work is to fabricate Al/p-Si photodetectors using TiO_2 and ZnO interlayers and investigate their performance for different values of illumination power at various wavelengths. The interlayers were fabricated by ALD, and the detection performance of the photodetectors was investigated by *I–V* and *I-t* measurements at different illumination power densities and wavelengths.

2. Experimental details

One-side polished p-type Si wafer with carrier concentrations of 7.3 $\times$ 10^{15} cm^{-3} and (100) orientation was used to fabricate TiO_2 and ZnO interlayers based Schottky-type photodetectors. The wafer cleaning procedure was realized by ultrasonication in acetone, deionized water and isopropanol solvents after slicing of wafer 1 $\times$ 2 cm^2 pieces. A HF: H_2O (1:10) solution was employed to remove undesired oxide layer by submerging the pieces into solution for only 30 s. 200 nm thick Al layers were evaporated on the back side of the pieces, and then the pieces were annealed at 450 °C in the N_2 filled oven for a couple of minutes to achieve ohmic contacts. The work functions of p-Si and Al are very close in energy and annealing is sufficient to compose an ohmic contact between Al and p-Si [28]. The pieces were separately transferred into Savannah S300 ALD system to grow TiO_2 (4 nm) and ZnO (4 nm) layers on the polished side of the pieces by adjusting the substrate temperature and deposition rate as 200 °C and 2 Å per cycle, respectively with titanium tetrachloride for TiO_2 precursor and diethyl zinc for ZnO precursor. The ALD system was used to precisely control the thickness of the TiO_2 and ZnO according to literature [29,30]. Both the TiO_2/p-Si and ZnO/p-Si sandwiches immediately were transferred into thermal evaporator to obtain 7.85 $\times$ 10^{-3} cm^2 area Al metallic contacts (100 nm) on the top of TiO_2 and ZnO layers with a hole array mask. The schematic illustration and measurement system of the Al/TiO_2/p-Si and Al/ZnO/p-Si photodetectors are shown in Fig. 1.

Schematic energy-band diagram of the Al/TiO_2/p-Si and Al/ZnO/p-Si heterojunction photodetector under illumination of light have been illustrated in Fig. 2a and b, respectively. Here, E_g, E_v, E_c, E_F, E_{vac} and χ indicate band gap energy, top of the valence band, bottom of the conduction band, Fermi level, the vacuum level and electron affinity, respectively. For this diagram, the band gap energy of TiO_2, ZnO and p-Si were taken as 3.2 eV, 3.37 eV, 1.12 eV respectively [31,32]. Electron affinities were assumed to be $\chi(TiO_2) = 4.10$ eV [32], $\chi(ZnO) = 4.35$ eV and $\chi(Si) = 4.05$ eV [31], respectively. Valence band offset (ΔE_v) and conduction band offset (ΔE_c) of the Si/TiO_2 heterostructure can be calculated as 2.31 eV and 0.05 eV, respectively [33]. In the case of the Si/ZnO heterostructure, the ΔE_v and ΔE_c were calculated as ΔE_v 2.55 eV and 0.3 eV, respectively [31].

Morphology and chemical compositions of the TiO_2 and ZnO interlayers were investigated by a ZEISS EVO LS10 SEM equipped with an EDX detector. *I–V* and *I-t* measurements of the photodetectors for various illumination power densities at different wavelengths were performed using a Frytronix FY-7000 solar simulator equipped with suitable filters.

3. Results and discussion

SEM images and EDX spectra with fast mapping images were obtained to characterize TiO_2 and ZnO interlayers. Fig. 3a and b show surface images of the TiO_2 and ZnO interlayers, and Fig. 3c and d shows fast mapping images. Surface morphologies of the interlayers are smooth and homogeneous. According to fast mapping of the interlayers, the atomic distribution of the TiO_2 and ZnO interlayers have homogenous pattern. These interlayers can be employed for Schottky-type photodetectors. EDX spectra of the TiO_2 and ZnO interlayers have been shown in Fig. 3e and f, respectively with atomic ratios of the elements. The EDX spectra confirm the synthesis of the TiO_2 and ZnO interlayers.

I–V characteristics of a photodetector give information about the relation between applied voltage and induced current for reverse and forward biases. ln*I-V* graphs of the Al/TiO_2/p-Si and Al/ZnO/p-Si photodetectors have been illustrated in Fig. 4a and b for increasing light power density, respectively. The insets of Fig. 4a and b show normal *I–V* characteristics curves for Al/TiO_2/p-Si and Al/ZnO/p-Si. According to *I–V* characteristics, the fabricated heterostructures exhibited photodetector behavior due to increasing current under illumination at reverse as well as forward biases. The increase of the current at -3V changed from 6.14 $\times$ 10^{-5} A to 1.49 $\times$ 10^{-4} A by increasing of light power density from dark to 100 mW/cm^2 for Al/TiO_2/p-Si photodetector. The current increased from 3.59 $\times$ 10^{-5} A to 2.86 $\times$ 10^{-4} A for Al/ZnO/p-Si photodetector in same condition. Thus, the photocurrents (I_{light} - I_{dark}) of the Al/TiO_2/p-Si and Al/ZnO/p-Si photodetectors were obtained as 8.76 $\times$ 10^{-5} and 2.50 $\times$ 10^{-4}, respectively. These photocurrent values can be comparable with literature for Schottky-type photodetector with TiO_2 and ZnO interlayers [34,35]. Furthermore, the ratio of photocurrent to dark currents for the Al/TiO_2/p-Si and Al/ZnO/p-Si photodetectors were calculated as 1.43 and 6.96, respectively.

By using of $R_j = dV/dI$ formalism, junction resistance (R_j) can be extracted from *I–V* characteristics, and shunt (R_{sh}) and series resistance (R_s) values are evaluated according to performance [36]. While the R_{sh} is obtained for reverse biases, R_s is obtained for forward biases, and high

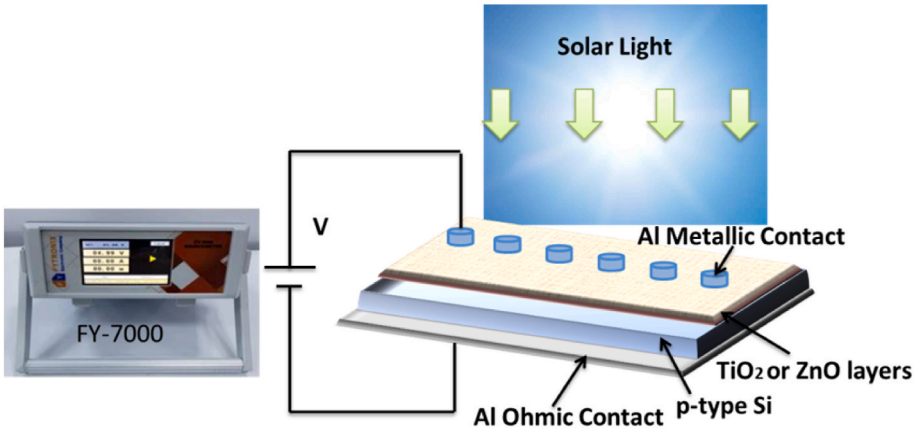

Fig. 1. Schematic representation of measurement system and structure of the fabricated photodetectors.

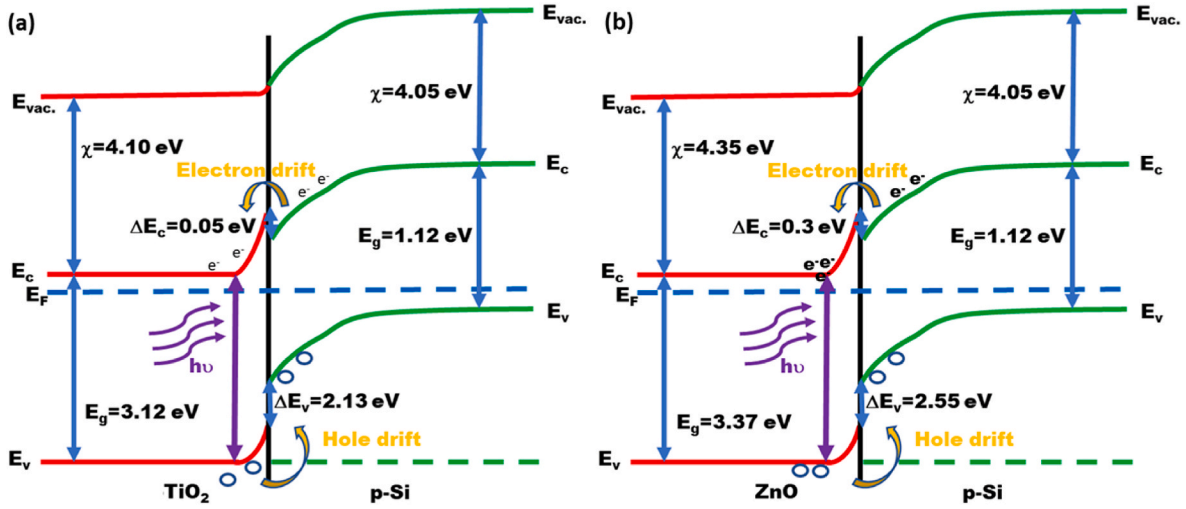

Fig. 2. Schematic energy-band diagram of **a)** Al/TiO_2/p-Si and **b)** Al/ZnO/p-Si heterojunction photodetectors under illumination of light.

R_{sh} and low R_s values are desired for good performance of the optoelectronic devices [37,67]. While the R_{sh} values are around 10^6 for both detectors, the R_s values are around 10^4 Ω and 10^3 Ω levels for Al/TiO_2/p-Si and Al/ZnO/p-Si photodetectors, respectively. Furthermore, Ocaya and Yakuphanoglu recently proposed that R_s were affected exponentially by the change of incident light with a constant rate of illumination power [38]. Our results confirmed this change by illumination power measurements.

I–V characteristics can help to calculate various diode parameters, which are important for the photodetection or photovoltaic performance, such as barrier height (Φ_b), series resistance (R_s) and ideality factor (n). These parameters can be calculated by various approximations according to literature [39]. One of them is thermionic emission theory, and it uses second linear region of the *I–V* characteristics for forward biases to determine both ideality factor and barrier height values. These regions were marked in Fig. 4a and b by using pointers [40]. According to this method current (I) is calculated by following formula:

$$I = I_0 \exp\left(\frac{qV}{nkT}\right)\left[1 - \exp\left(-\frac{qV}{kT}\right)\right] \quad (1)$$

where I_0 is saturation current. k, q and V are Boltzmann's constant, charge of electron and the applied bias voltage, respectively. The I_0 is given by:

$$I_0 = AA^*T^2 \exp\left(-\frac{q\Phi_b}{kT}\right) \quad (2)$$

where A^*, A and T are Richardson constant (32 A/K^2.cm^2 for p-Si), diode area ($A = 7.85 \times 10^{-3}$ cm^2) and the temperature, respectively. The n and Φ_b are given following equation for $V \geq 3kT/q$ region:

$$n = \frac{q}{kT}\left(\frac{dV}{dlnI}\right) \quad (3)$$

$$\Phi_b = \frac{kT}{q} ln\left(\frac{A^*AT^2}{I_0}\right) \quad (4)$$

The calculated ideality factor and barrier height values have been listed in Table 1 for Al/TiO_2/p-Si and Al/ZnO/p-Si photodetectors. Both photodetectors have higher n values than unity because of the large number of traps or interface states of the heterostructures [41]. These high values of n can be attributed to non-ideal diode structure, interfacial layer of TiO_2 and ZnO and barrier inhomogeneity [13]. The changes of the n and Φ_b by power illumination density have been shown in Fig. 5a and b. Both photodetectors have generally same decreasing Φ_b and increasing n profiles. The changes at the n and Φ_b values are clearly confirmed that they are function of light power density for both photodetectors.

Rectifying ratio (*RR*) is the ratio of the forward bias current to reverse bias current at same positive and negative voltages [42]. The *RR* values were calculated for both Al/TiO_2/p-Si and Al/ZnO/p-Si photodetectors. Fig. 6a and b show changing profiles of the *RR* values depending on power density of illumination for Al/TiO_2/p-Si and Al/ZnO/p-Si photodetectors, respectively. While the *RR* values of Al/TiO_2/p-Si almost stayed constant at about 4.0, *RR* values of Al/ZnO/p-Si photodetector decreased to around 4.0 after 20 mW/cm^2. These results clearly revealed that both photodetectors almost have stable *RR* values against to increasing light power. In the literature, the *RR* values of Schottky-type photodetectors usually decrease with increasing light power [43,44]. However, here the *RR* values stayed constant by changing light power due to the fact that illumination caused an increase of current for both reverse and forward biases. This result highlighted that the fabricated devices have enough response under illumination in forward and reverse biases for same voltage value. This can be attributed to photovoltaic behavior of the devices [45].

Norde proposed another method to determine R_s and Φ_b values from forward bias *I–V* curve [46]. The detailed explanation about the method and Norde function can be found in literature [47,48]. The Norde function is given by following formula:

$$F(V) = \frac{V}{\gamma} - \frac{kT}{q} ln\left(\frac{I(V)}{AA^*T^2}\right) \quad (5)$$

where γ is minimum integer value higher than n value of thermionic emission. The $I(V)$ is the voltage dependent current. The Φ_b and R_s are obtained by following formula after rearranging of Norde function:

$$\Phi_b = F(V_0) + \left[\frac{V_0}{\gamma} - \frac{kT}{q}\right] \quad (6)$$

$$R_s = \frac{\gamma - n}{I}\frac{kT}{q} \quad (7)$$

where V_0 is minimum voltage related to $F(V)$ function.

Fig. 7a and b display Norde function plots of the Al/TiO_2/p-Si and Al/ZnO/p-Si photodetectors, respectively. The photodetectors exhibited normal Norde function plots, and calculated R_s and Φ_b values were tabulated in Table 1 for both photodetectors. The obtained Φ_b values of 0.65 eV and 0.72 eV are close to Φ_b values of TE method for Al/TiO_2/p-Si and Al/ZnO/p-Si. The R_s values of both photodetectors are good agreement by R_s values calculated from R_j.

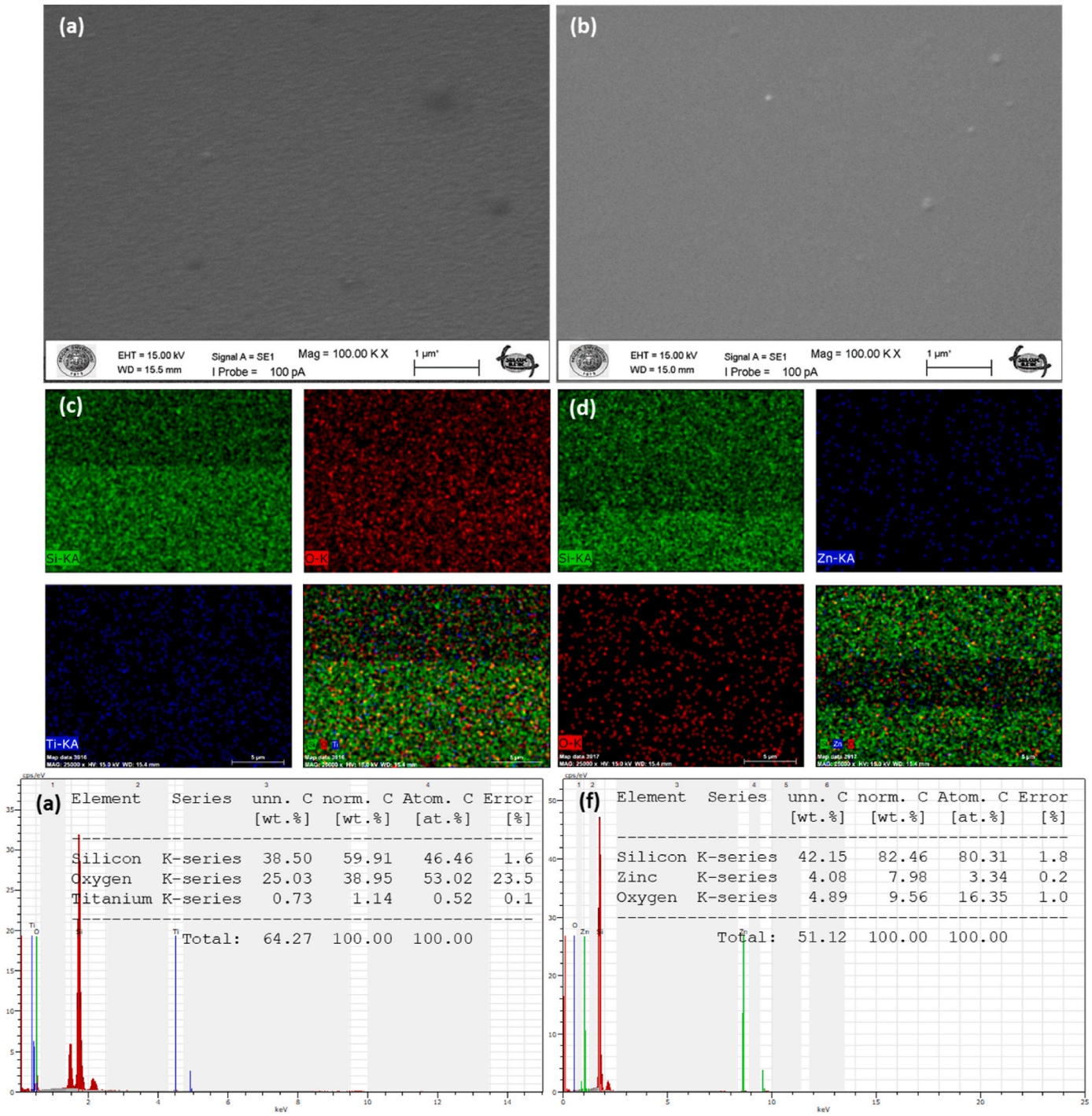

Fig. 3. SEM images of the a) TiO_2 and b) ZnO, fast mapping of c) TiO_2 and d) ZnO, and EDX spectra of e) TiO_2 and f) ZnO interlayers.

Cheung and Cheung introduced another method to calculate the n, Φ_b and R_s values from I–V curve [49]. Cheung method describes current by following equation:

$$I = I_0 \exp\left(\frac{q(V - IR_s)}{nkT}\right) \tag{8}$$

where IR_s shows voltage drops related to series resistance of junction. The Cheung's functions can be extracted from current and given by following formulas:

$$\frac{dV}{d(\ln I)} = IR_s + n\frac{kT}{q} \tag{9}$$

$$H(I) = V - n\left(\frac{kT}{q}\right)\ln\left(\frac{I}{AA^*T^2}\right) \tag{10}$$

where $H(I)$ can be rearranged by following equation:

$$H(I) = IR_s + n\Phi_b \tag{11}$$

Plotting of $dV/d(\ln I)$ versus I provides to determine ideality factor and one of the series resistance values, and $H(I)$ versus I graph gives barrier height and another series resistance. These two separate R_s values should be close each other to confirm the accuracy of the method [50]. Fig. 8a and b show Cheung function plots of the Al/TiO_2/p-Si and Al/ZnO/p-Si photodetectors, respectively. The determined n, Φ_b and R_s

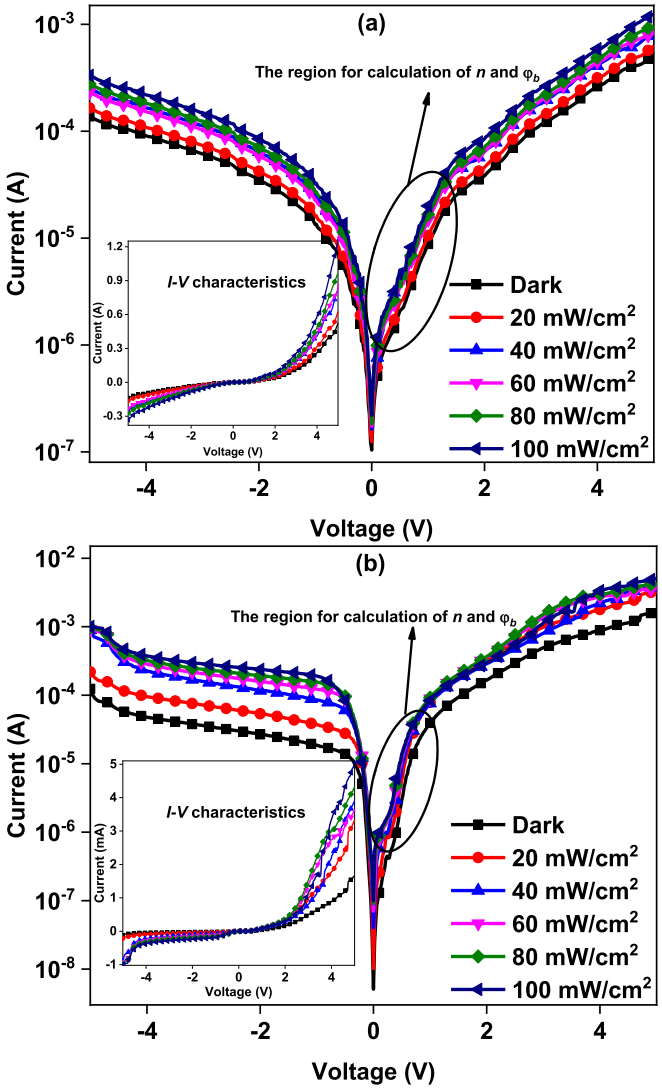

Fig. 4. ln*I-V* plots of the as well as *I–V* curves (insets) of the **a)** Al/TiO_2/p-Si and **b)** Al/ZnO/p-Si photodetectors for changing light power density.

values were listed in Table 1. The discrepancy from linearity at the Cheung plots can be attributed to barrier inhomogeneity of TiO_2 and ZnO interlayers [51].

The photocurrent transient (*I-t*) measurements show the response speed of the photodetectors for changing light-on and light-off modes [52]. It is important to estimate responsivity, photosensitivity and detectivity characteristics as well as switching speed. Fig. 9a and b display *I-t* plots of the Al/TiO_2/p-Si and Al/ZnO/p-Si photodetectors, respectively for 5 s with light-on and 5 s with light-off. Both photodetectors exhibited a linear increase of the photocurrent with illumination power. However, the Al/ZnO/p-Si photodetector has higher photocurrent levels for all power density levels.

The photocurrent (I_p), photosensitivity (K), responsivity (R) and specific detectivity (D^*) formulas are given by following equations [53].

$$I_p = I_{light} - I_{dark} \tag{12}$$

$$K = \frac{I_p}{I_{dark}} \tag{13}$$

$$R = \frac{I_p}{PA} \tag{14}$$

$$D^* = R\sqrt{\frac{A}{2qI_{dark}}} \tag{15}$$

where P is the illumination power, A is the effective area of detector, and q is charge of electrons.

Fig. 10a and b illustrate photosensitivity changes of the Al/TiO_2/p-Si and Al/ZnO/p-Si photodetectors depending on light power density. The K values increased with increment of power almost linearly for Al/TiO_2/p-Si photodetector. However, Al/ZnO/p-Si photodetector increased up to 1744 for 60 mW/cm^2 and then decreased to 342 for 100 mW/cm^2. These changes can be attributed to fast recombination of the carriers for ZnO based photodetector due to the large number of traps at the interface.

Fig. 11a and b exhibit light power density dependent responsivity profiles of the Al/TiO_2/p-Si and Al/ZnO/p-Si photodetectors, respectively. While the Al/TiO_2/p-Si photodetector has increasing responsivity profile from 5.53 mA/W to 21.7 mA/W, the Al/ZnO/p-Si photodetector has decreasing profile from 755 mA/W to 355 mA/W. Furthermore, the responsivity values of the Al/ZnO/p-Si photodetector are higher than the Al/TiO_2/p-Si photodetector.

Light power density dependent specific detectivity profiles of the Al/TiO_2/p-Si and Al/ZnO/p-Si photodetectors have been shown in Fig. 12a and b, respectively. The detectivity values almost increased linearly for Al/TiO_2/p-Si photodetector, but Al/ZnO/p-Si photodetector exhibited fluctuations depending on light power density. These kinds of characteristics at the photodetectors can be attributed to increasing or decreasing dark current due to defect states in the interfacial layers of TiO_2 and ZnO [54]. The Al/ZnO/p-Si photodetector has higher detectivity values than Al/TiO_2/p-Si photodetector. Its values are high enough for a kind of Schottky-type photodetector according to literature [55,56].

The Al/TiO_2/p-Si and Al/ZnO/p-Si photodetectors were compared with previous photodetectors in Table 2 in the case of photosensitivity, responsivity and detectivity performances. It can be concluded that the photodetection characteristics of both Al/TiO_2/p-Si and Al/ZnO/p-Si photodetectors are in good agreement with the literature (references shown in Table 2). These characteristics can be improved for photodetection applications or optoelectronic devices.

Figs. 13a and b show *I–V* characteristics of Al/TiO_2/p-Si and Al/ZnO/p-Si photodetectors for various wavelengths and fixed powers at reverse biases, respectively. The variation of the photocurrent as a function of the wavelength from UV to visible is attributed to the various absorption levels at the interface of the photodetectors [66].

Wavelength dependent *I*-t characteristics of the Al/TiO_2/p-Si and Al/ZnO/p-Si photodetectors were obtained to calculate photocurrent, photosensitivity, responsivity and detectivity values. Table 3 shows calculated detectors parameters for various wavelengths for Al/TiO_2/p-Si and Al/ZnO/p-Si photodetectors. Although the two detectors present different detector parameters, both the Al/TiO_2/p-Si and Al/ZnO/p-Si photodetectors have highest responsivity and detectivity values at

Table 1
The diode parameters of the Al/TiO_2/p-Si and Al/ZnO/p-Si photodetectors.

Device interlayer	Saturation Current (I_0)	n (TE) -	n Cheung -	Φ_b(TE) (eV)	Φ_b Cheung (eV)	Φ_b Norde (eV)	R_s Cheung (kΩ (H (I)))	R_s Cheung (kΩ (dln (I)))	R_s Norde (kΩ)
TiO_2	4.42×10^{-7}	12.71	12.73	0.64	0.68	0.65	5.22	4.78	3.47
ZnO	5.32×10^{-8}	4.80	4.85	0.69	0.78	0.72	3.38	2.94	6.26

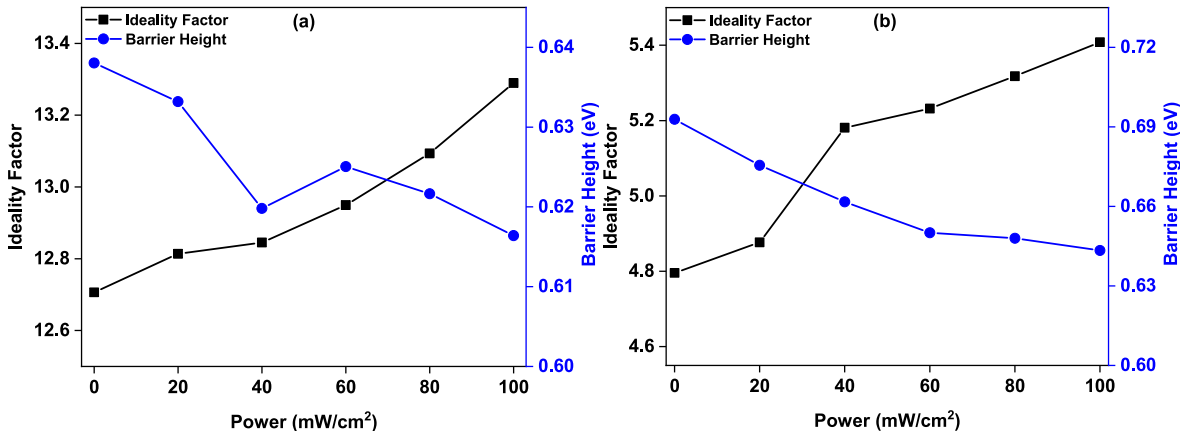

Fig. 5. Light power density dependent n - Φ_b profiles of the **a)** Al/TiO_2/p-Si and **b)** Al/ZnO/p-Si photodetectors.

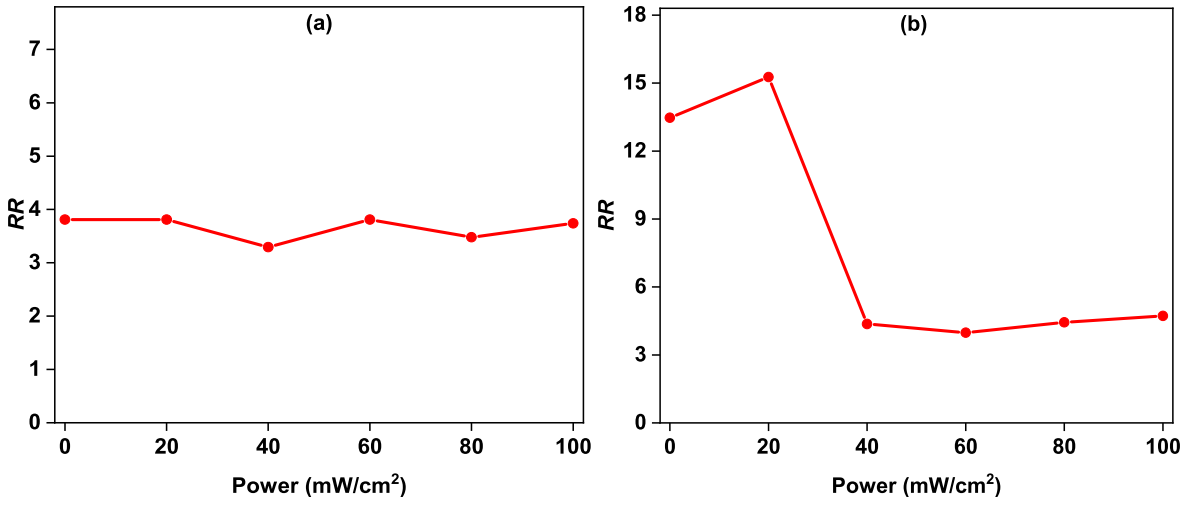

Fig. 6. *RR* versus light power density plots of **a)** Al/TiO_2/p-Si and **b)** Al/ZnO/p-Si photodetectors.

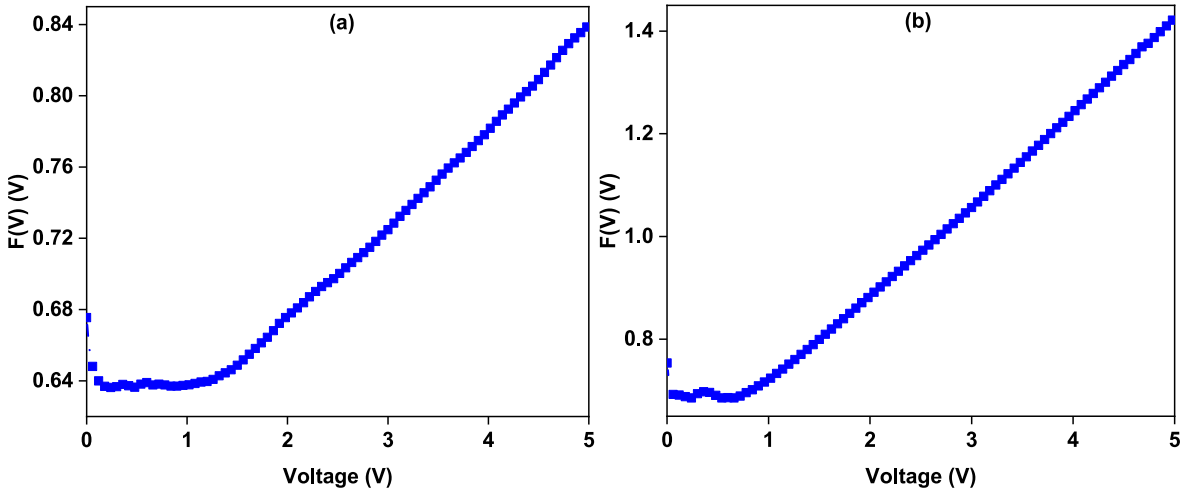

Fig. 7. *F(V)–V* plots of **a)** Al/TiO_2/p-Si and **b)** Al/ZnO/p-Si photodetectors.

600 nm wavelength. The Al/ZnO/p-Si photodetector exhibited better detection performance than Al/TiO_2/p-Si photodetector.

Fig. 14a and b show EQE plots of the Al/TiO_2/p-Si and Al/ZnO/p-Si photodetectors, respectively for the range of 351 nm and 800 nm wavelengths from the formula of EQE $= 1240 \times (R/\lambda) \times$ 100%. While the Al/ZnO/p-Si photodetector reached up 173.08% maximum EQE value at 550 nm, Al/TiO_2/p-Si photodetector at 7.31% at 600 nm wavelengths. Both photodetectors have good response to the visible light according to EQE spectrum, and they can be used in optoelectronic applications.

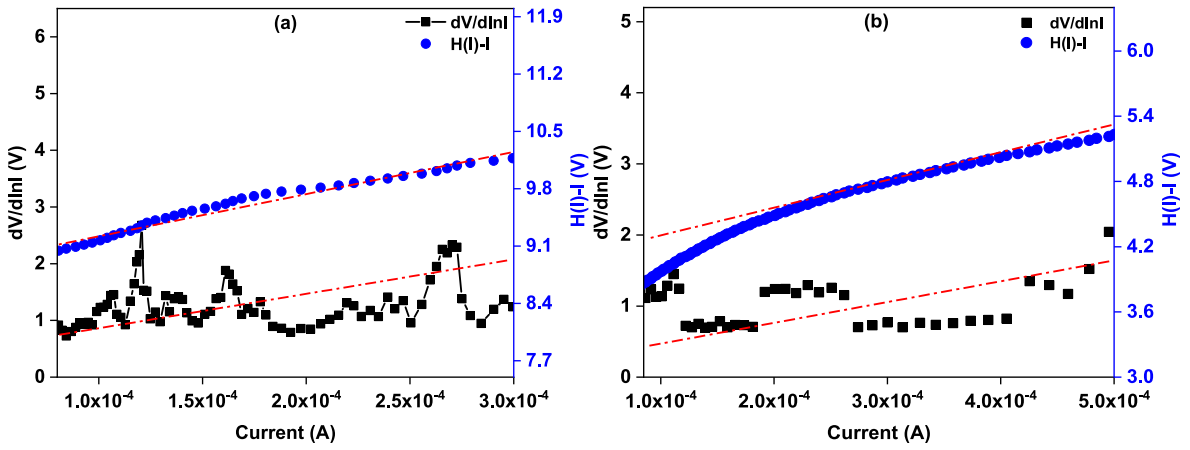

Fig. 8. Cheung plots of **a)** Al/TiO_2/p-Si and **b)** Al/ZnO/p-Si photodetectors.

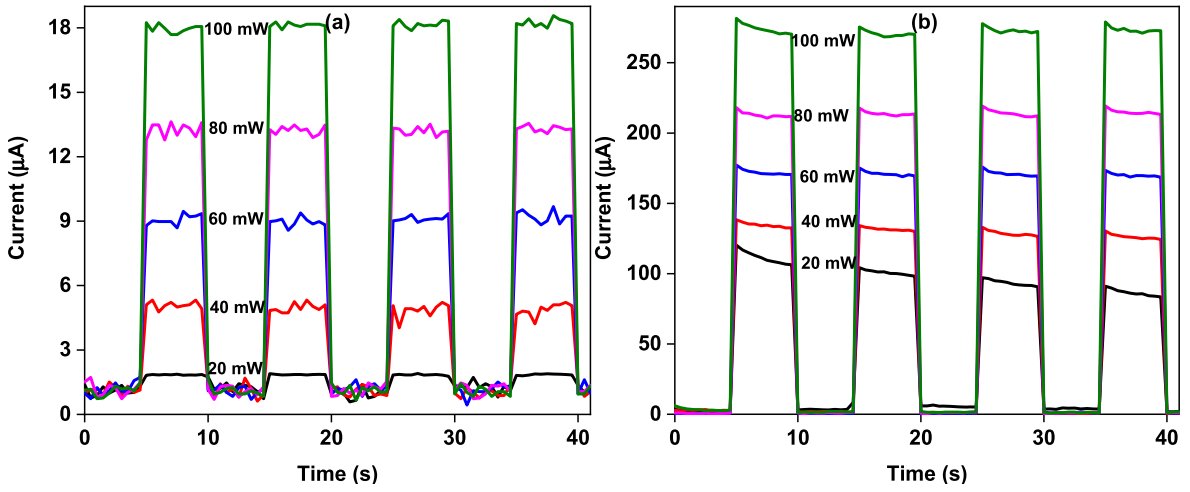

Fig. 9. *I-t* plots of **a)** Al/TiO_2/p-Si and **b)** Al/ZnO/p-Si photodetectors.

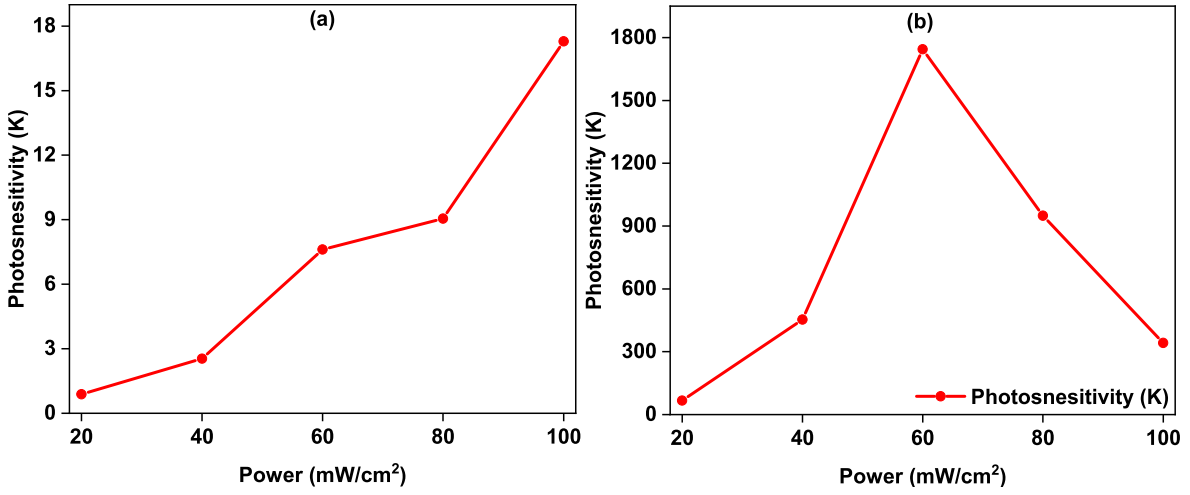

Fig. 10. Photosensitivity changes of **a)** Al/TiO_2/p-Si and **b)** Al/ZnO/p-Si photodetectors for different values of light power density.

4. Conclusion

TiO_2 and ZnO metal oxide interlayers were grown on p-Si by ALD technique to fabricate Schottky-type photodetectors of Al/TiO_2/p-Si and Al/ZnO/p-Si. The fabricated photodetectors were tested by *I–V* and *I-t* measurements for various light power densities and wavelengths. SEM and EDX analysis confirmed homogenous morphology and chemical composition of the TiO_2 and ZnO interlayers. The diode parameters of ideality factor, series resistance and barrier height values were determined with TE, Norde and Cheung methods. The Al/TiO_2/p-Si and Al/

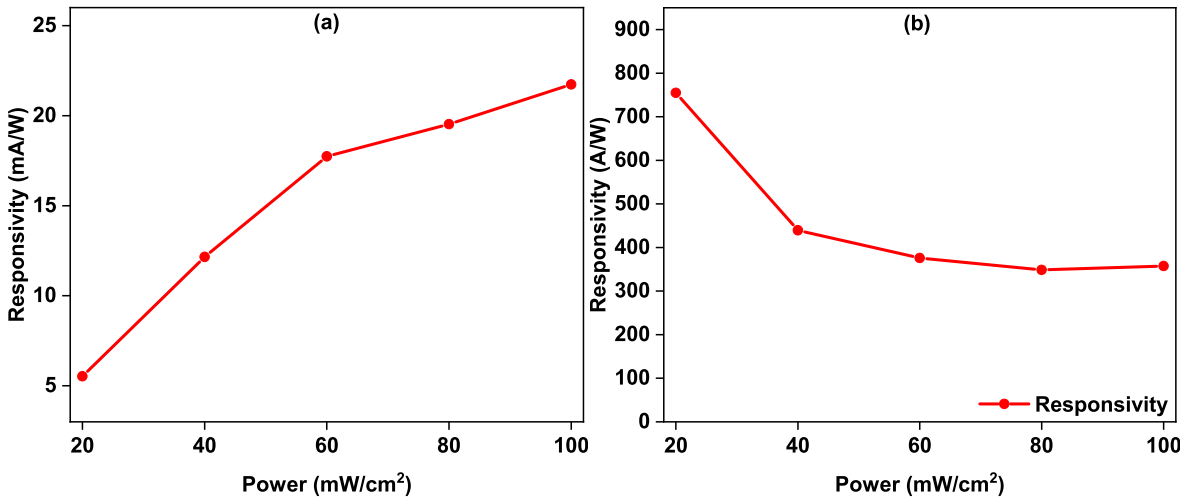

Fig. 11. Responsivity versus light power density plots of **a)** Al/TiO_2/p-Si and **b)** Al/ZnO/p-Si photodetectors.

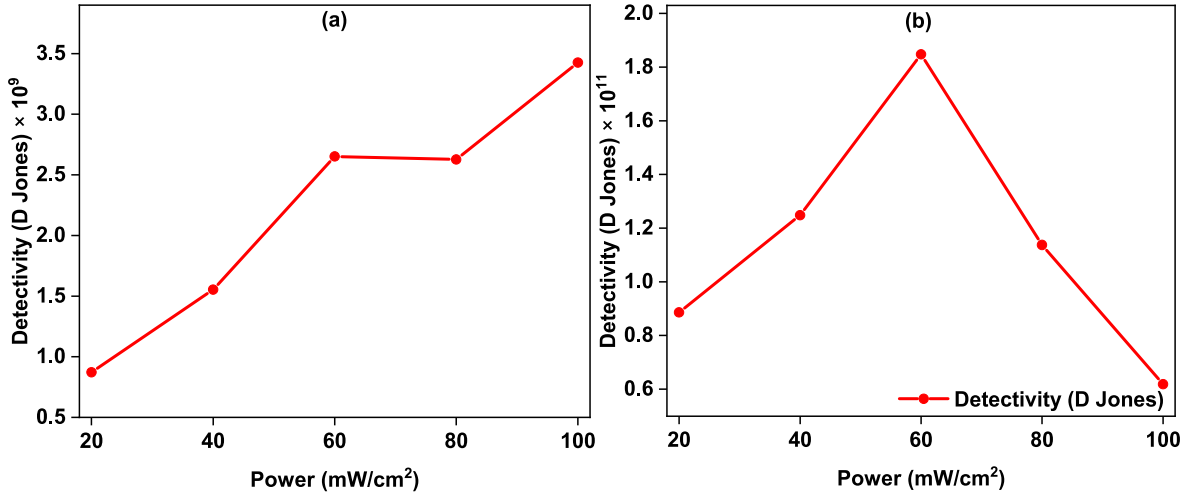

Fig. 12. Detectivity profile of **a)** Al/TiO_2/p-Si and **b)** Al/ZnO/p-Si photodetectors for changing light power density.

Table 2
Comparison of the Al/TiO_2/p-Si and Al/ZnO/p-Si photodetectors with previous works.

Device	Device Type	Wavelength (nm)	Photosensitivity (−)	Responsivity (A/W)	Detectivity (Jones)	Reference
ZnS:Mn/p-Si	Schottky	Visible	–	7.90×10^{-5}	3.50×10^{9}	[57]
ZnS/p-Si	MSM	UV	–	68.98×10^{-3}	4.29×10^{12}	[58]
In doped ZnO nanorods	MSM	390	–	2.50	1.44×10^{11}	[59]
Cu/ZnO/Cu	MSM	365	–	1.20	5.77×10^{11}	[60]
n-ZnO/p-ZnO	p-n	376	–	12.9	2.90×10^{9}	[61]
Cu/Yb@V_2O_5/n-Si	Schottky	–	55.45	0.04	9.97×10^{10}	[62]
Ag/TiO_2/Ag	MSM	365	–	2.14	6.01×10^{12}	[63]
Cu/TiO_2/FTO	Schottky	365	–	0.90	4.50×10^{12}	[64]
n-TiO_2/p-Si	Schottky	365	–	0.10	2.39×10^{9}	[65]
Al/TiO_2/p-Si	Schottky	Visible	17.29	0.02	3.43×10^{9}	This work
Al/ZnO/p-Si			1744	0.76	1.85×10^{11}	

ZnO/p-Si photodetectors have barrier height values of 0.64 eV and 0.69 eV, respectively. The photodetectors have exhibited high ideality factor values according to TE method. The photosensitivity, responsivity and detectivity values of the fabricated devices were obtained for changing light power density and wavelengths from UV to visible range of electromagnetic spectrum. While the Al/TiO_2/p-Si photodetector have 21.7 mA/W responsivity value, the Al/ZnO/p-Si photodetector have 755 mA/W responsivity. The Al/ZnO/p-Si photodetector exhibited high EQE value of 173.08%. Both photodetectors have response within the visible spectrum. According to performance results, Al/ZnO/p-Si exhibited better photodetector performance than Al/TiO_2/p-Si.

CRediT authorship contribution statement

D. Esra Yıldız: Supervision, Writing - review & editing. **Adem Kocyigit:** Writing – original draft, Writing – review & editing. **Murat Yıldırım:** Data curation, Methodology, Writing - review & editing.

Table 3
Various detection parameters of the Al/TiO_2/p-Si and Al/ZnO/p-Si photodetectors for various wavelengths.

Detector	Wavelength(nm)	Photocurrent (A)	Photosensitivity –	Responsivity (A/W)	Specific detectivity (Jones)
Al/TiO_2/p-Si	351	2.70×10^{-6}	7.95	0.011	2.98×10^{9}
	400	4.05×10^{-6}	11.77	0.018	4.92×10^{9}
	450	5.06×10^{-6}	15.12	0.019	5.13×10^{9}
	500	5.56×10^{-6}	15.29	0.026	6.81×10^{9}
	550	6.22×10^{-6}	16.90	0.032	8.19×10^{9}
	600	7.22×10^{-6}	19.53	0.035	9.12×10^{9}
	650	7.48×10^{-6}	20.23	0.030	7.67×10^{9}
	700	5.47×10^{-6}	14.79	0.028	7.18×10^{9}
	750	4.55×10^{-6}	12.31	0.022	5.74×10^{9}
	800	3.57×10^{-6}	9.65	0.016	4.04×10^{9}
Al/ZnO/p-Si	351	1.17×10^{-4}	38.61	0.482	4.33×10^{10}
	400	1.22×10^{-4}	35.35	0.553	4.67×10^{10}
	450	1.31×10^{-4}	39.15	0.490	4.20×10^{10}
	500	1.40×10^{-4}	38.46	0.660	5.42×10^{10}
	550	1.51×10^{-4}	40.90	0.768	6.27×10^{10}
	600	1.65×10^{-4}	44.55	0.807	6.58×10^{10}
	650	1.69×10^{-4}	45.68	0.673	5.48×10^{10}
	700	1.46×10^{-4}	39.52	0.745	6.07×10^{10}
	750	1.38×10^{-4}	37.39	0.678	5.52×10^{10}
	800	1.29×10^{-4}	39.36	0.565	4.90×10^{10}

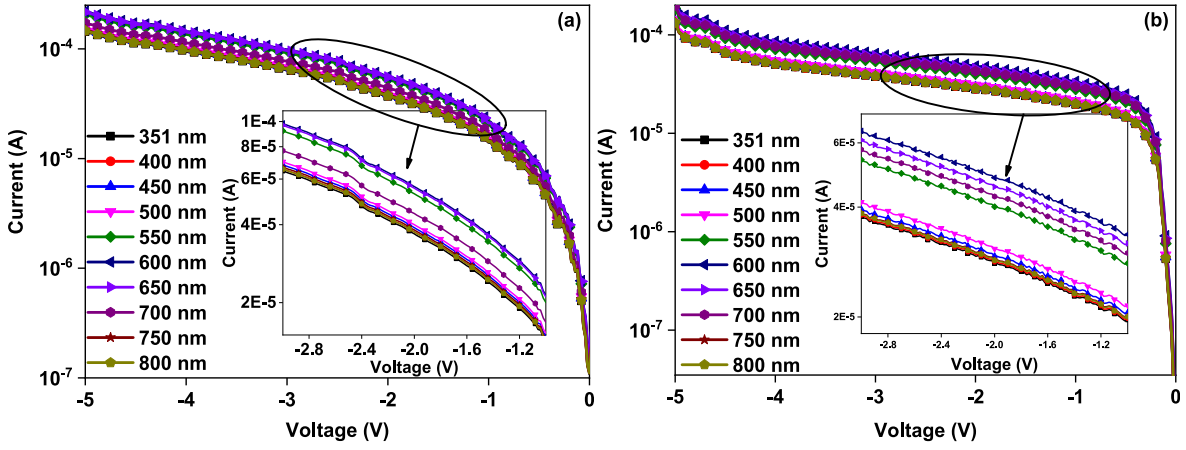

Fig. 13. *I–V* characteristics of **a)** Al/TiO_2/p-Si and **b)** Al/ZnO/p-Si photodetectors for various wavelengths.

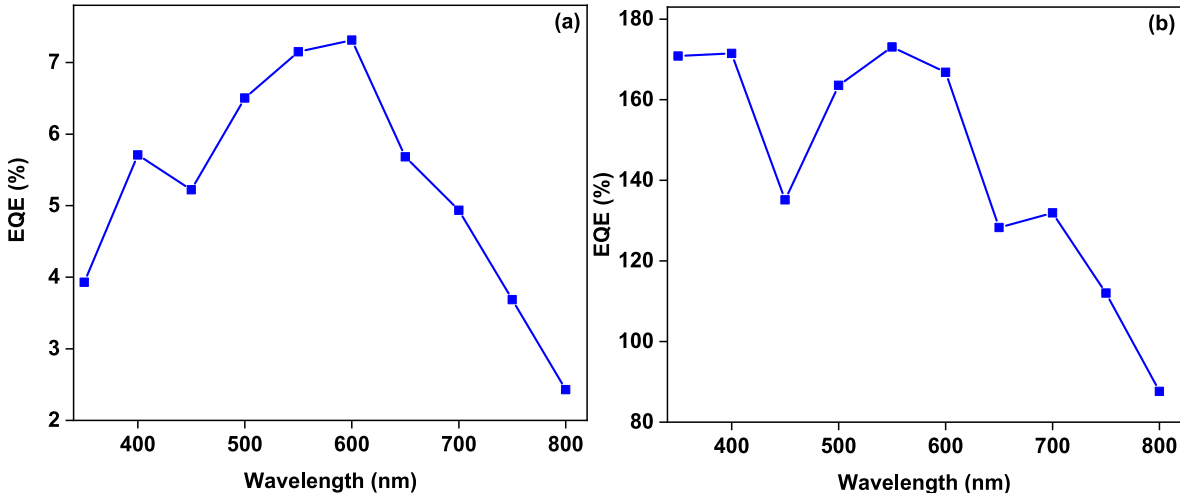

Fig. 14. EQE profiles of **a)** Al/TiO_2/p-Si and **b)** Al/ZnO/p-Si photodetectors in the range of 350–800 nm.

Declaration of competing interest

The authors declare that they have no known competing financial interests or personal relationships that could have appeared to influence the work reported in this paper.

Data availability

Data will be made available on request.

References

[1] C. Brecher, A. Müller, Y. Dassen, S. Storms, Automation technology as a key component of the Industry 4.0 production development path, Int. J. Adv. Manuf. Technol. 117 (2021) 2287–2295, https://doi.org/10.1007/s00170-021-07246-5.

[2] S.C. Arum, D. Grace, P.D. Mitchell, A review of wireless communication using high-altitude platforms for extended coverage and capacity, Comput. Commun. 157 (2020) 232–256, https://doi.org/10.1016/j.comcom.2020.04.020.

[3] F. Xia, Wireless sensor technologies and applications, Sensors 9 (2009) 8824–8830, https://doi.org/10.3390/s91108824.

[4] M. Majid, S. Habib, A.R. Javed, M. Rizwan, G. Srivastava, T.R. Gadekallu, J.C. W. Lin, Applications of wireless sensor networks and internet of things frameworks in the industry revolution 4.0: a systematic literature review, Sensors 22 (2022) 2087, https://doi.org/10.3390/s22062087.

[5] Z. Bielecki, K. Achtenberg, M. Kopytko, J. Mikołajczyk, J. Wojtas, A. Rogalski, Review of photodetectors characterization methods, Bull. Pol. Acad. Sci. Tech. Sci. 70 (2022) 1–26, https://doi.org/10.24425/bpasts.2022.140534.

[6] C. Yang, G. Wang, M. Liu, F. Yao, H. Li, Mechanism, material, design, and implementation principle of two-dimensional material photodetectors, Nanomaterials 11 (2021) 2688, https://doi.org/10.3390/nano11102688.

[7] J. Jiang, Y. Wen, H. Wang, L. Yin, R. Cheng, C. Liu, L. Feng, J. He, Recent advances in 2D materials for photodetectors, Adv. Electron. Mater. 7 (2021), 2001125, https://doi.org/10.1002/aelm.202001125.

[8] C. Liu, J. Guo, L. Yu, J. Li, M. Zhang, H. Li, Y. Shi, D. Dai, Silicon/2D-material photodetectors: from near-infrared to mid-infrared, Light Sci. Appl. 10 (2021) 1–21, https://doi.org/10.1038/s41377-021-00551-4.

[9] M. Malik, M.A. Iqbal, J.R. Choi, P.V. Pham, 2D materials for efficient photodetection: overview, mechanisms, performance and UV-IR range applications, Front. Chem. 10 (2022) 488, https://doi.org/10.3389/fchem.2022.905404.

[10] Y. Gao, J. Xu, S. Shi, H. Dong, Y. Cheng, C. Wei, X. Zhang, S. Yin, L. Li, TiO2 nanorod arrays based self-powered UV photodetector: heterojunction with NiO nanoflakes and enhanced UV photoresponse, ACS Appl. Mater. Interfaces 10 (2018) 11269–11279, https://doi.org/10.1021/acsami.7b18815.

[11] M. Nicolaescu, C. Bandas, C. Orha, V. Şerban, C. Lazău, S. Căprărescu, Fabrication of a uv photodetector based on n-tio2/p-cumno2 heterostructures, Coatings 11 (2021) 1380, https://doi.org/10.3390/coatings11111380.

[12] S.I. Inamdar, V.V. Ganbavle, K.Y. Rajpure, ZnO based visible-blind UV photodetector by spray pyrolysis, Superlattice. Microst. 76 (2014) 253–263, https://doi.org/10.1016/j.spmi.2014.09.041.

[13] I. Orak, A. Kocyigit, A. Turut, The surface morphology properties and respond illumination impact of ZnO/n-Si photodiode by prepared atomic layer deposition technique, J. Alloys Compd. 691 (2017) 873–879, https://doi.org/10.1016/j.jallcom.2016.08.295.

[14] M. Yıldırım, A. Kocyigit, Characterization of Al/In:ZnO/p-Si photodiodes for various in doped level to ZnO interfacial layers, J. Alloys Compd. 768 (2018) 1064–1075, https://doi.org/10.1016/j.jallcom.2018.07.295.

[15] M.O. Erdal, M. Yıldırım, A. Kocyigit, A comparison of the electrical characteristics of TiO2/p-Si/Ag, GNR-TiO2/p-Si/Ag and MWCNT-TiO2/p-Si/Ag photodiodes, J. Mater. Sci. Mater. Electron. 30 (2019) 13617–13626, https://doi.org/10.1007/s10854-019-01731-0.

[16] D. Banerjee, I.M. Asuo, A. Pignolet, S.G. Cloutier, Low-cost photodetector architectures fabricated at room-temperature using nano-engineered silicon wafer and sol-gel TiO2 – based heterostructures, Sci. Rep. 9 (2019) 1–9, https://doi.org/10.1038/s41598-019-54481-8.

[17] G. Chatzigiannakis, A. Jaros, R. Leturcq, J. Jungclaus, T. Voss, S. Gardelis, M. Kandyla, Laser-microstructured ZnO/p-Si photodetector with enhanced and Broadband responsivity across the ultraviolet-visible-near-infrared range, ACS Appl. Electron. Mater. 2 (2020) 2819–2828, https://doi.org/10.1021/acsaelm.0c00492.

[18] S. Sahare, R.K. Choubey, G. Jadhav, T.M. Bhave, S. Mukherjee, S. Kumar, A comparative investigation of optical and structural properties of Cu-doped CdO-derived nanostructures, J. Supercond. Nov. Magn. 30 (2017) 1439–1446, https://doi.org/10.1007/s10948-016-3943-y.

[19] S. Gupta, A. Kumar, S. Mukherjee, K.K. Kushwah, S.K. Mahobia, P. Patharia, A. Kushwaha, D. Yadav, U.K. Dwivedi, S. Kumar, R.K. Choubey, Temperature-dependent study of the fabricated ZnS/p-Si heterojunction, Phys. B Condens. Matter 657 (2023), 414831, https://doi.org/10.1016/j.physb.2023.414831.

[20] J.K. Saha, R.N. Bukke, N.N. Mude, J. Jang, Significant improvement of spray pyrolyzed ZnO thin film by precursor optimization for high mobility thin film transistors, Sci. Rep. 10 (2020) 1–11, https://doi.org/10.1038/s41598-020-65938-6.

[21] B. Endrődi, E. Kecsenovity, K. Rajeshwar, C. Janáky, One-step electrodeposition of nanocrystalline TiO2 films with enhanced photoelectrochemical performance and charge storage, ACS Appl. Energy Mater. 1 (2018) 851–858, https://doi.org/10.1021/acsaem.7b00289.

[22] P.O. Oviroh, R. Akbarzadeh, D. Pan, R.A.M. Coetzee, T.C. Jen, New development of atomic layer deposition: processes, methods and applications, Sci. Technol. Adv. Mater. 20 (2019) 465–496, https://doi.org/10.1080/14686996.2019.1599694.

[23] M. Yıldırım, A. Kocyigit, Y. Torlak, E. Yenel, A.A. Hussaini, M. Kuş, Electrical behaviors of the Co- and Ni-based POMs interlayered Schottky photodetector devices, Adv. Mater. Interfac. 9 (2022), 2102304, https://doi.org/10.1002/admi.202102304.

[24] S. Zhou, X. Peng, H. Liu, Z. Zhang, L. Ye, H. Li, Y. Xiong, L. Niu, F. Chen, L. Fang, C. Kong, W. Li, X. Yang, H. Zhang, High-performance β-Ga 2 O 3 -based solar-blind photodetector with ultralow dark current and fast photoresponse for deep-ultraviolet communication, Opt. Mater. Express 12 (2022) 327, https://doi.org/10.1364/ome.449496.

[25] A. Kaya, E. Marıl, Ş. Altındal, İ. Uslu, The comparative electrical characteristics of Au/n-Si (MS) diodes with and without a 2% graphene cobalt-doped Ca3Co4Ga0.001Ox interfacial layer at room temperature, Microelectron. Eng. 149 (2016) 166–171, https://doi.org/10.1016/J.MEE.2015.10.012.

[26] J. Gulomov, O. Accouche, R. Aliev, R. Ghandour, I. Gulomova, Investigation of N-ZnO/p-Si and N-TiO2/p-Si Heterojunction Solar Cells: TCAD+DFT, IEEE Access, 2023, https://doi.org/10.1109/ACCESS.2023.3268033.

[27] S. Hernández, D. Hidalgo, A. Sacco, A. Chiodoni, A. Lamberti, V. Cauda, E. Tresso, G. Saracco, Comparison of photocatalytic and transport properties of TiO2 and ZnO nanostructures for solar-driven water splitting, Phys. Chem. Chem. Phys. 17 (2015) 7775–7786, https://doi.org/10.1039/c4cp05857g.

[28] H.C. Card, Aluminum-Silicon Schottky barriers and ohmic contacts in integrated circuits, IEEE Trans. Electron. Dev. 23 (1976) 538–544, https://doi.org/10.1109/T-ED.1976.18449.

[29] S.H.K. Park, Y.E. Lee, Controlling preferred orientation of ZnO thin films by atomic layer deposition, J. Mater. Sci. 39 (2004) 2195–2197, https://doi.org/10.1023/B:JMSC.0000017786.81842.ae.

[30] H.-E. Cheng, C.-M. Hsu, Y.-C. Chen, Substrate materials and deposition temperature dependent growth characteristics and photocatalytic properties of ALD TiO2 films, J. Electrochem. Soc. 156 (2009) D275, https://doi.org/10.1149/1.3138723.

[31] F.Z. Bedia, A. Bedia, D. Kherbouche, Electrical properties of ZnO/p-Si heterojunction for solar cell application, Int. J. Mater. Eng. 2013 (2013) 59–65, https://doi.org/10.5923/J.IJME.20130304.01.

[32] J.Z. Chen, T.H. Chen, L.W. Lai, P.Y. Li, H.W. Liu, Y.Y. Hong, D.S. Liu, Preparation and characterization of surface photocatalytic activity with NiO/TiO2 nanocomposite structure, Materials 8 (2015) 4273–4286, https://doi.org/10.3390/ma8074273.

[33] A. Dewasi, A. Mitra, UV–visible light detection with TiO2 thin film deposited on chemically textured p-Si substrate, J. Mater. Sci. Mater. Electron. 29 (2018) 9209–9217, https://doi.org/10.1007/S10854-018-8949-8/FIGURES/8.

[34] H.Y. Lee, M.Y. Chern, Optical properties of ITO/ZnO Schottky diode with enhanced UV Photoresponse, J. Kor. Phys. Soc. 67 (2015) 1804–1808, https://doi.org/10.3938/jkps.67.1804.

[35] G.M. Ali, Performance analysis of planar Schottky photodiode based on nanostructured ZnO thin film grown by three different techniques, J. Alloys Compd. 831 (2020), 154859, https://doi.org/10.1016/j.jallcom.2020.154859.

[36] L.D. Rao, V.R. Reddy, Electrical parameters and series resistance analysis of Au/Y/p-InP/Pt Schottky barrier diode at room temperature, in: AIP Conf. Proc., AIP Publishing LLC, 2016, 120020, https://doi.org/10.1063/1.4948092.

[37] A. Koçyiğit, A. Sarılmaz, T. Öztürk, F. Ozel, M. Yıldırım, A Au/CuNiCoS4/p-Si photodiode: electrical and morphological characterization, Beilstein J. Nanotechnol. 12 (2021) 984–994, https://doi.org/10.3762/bjnano.12.74.

[38] R.O. Ocaya, F. Yakuphanoğlu, Ocaya–Yakuphanoğlu method for series resistance extraction and compensation of Schottky diode I–V characteristics, Meas. J. Int. Meas. Confed. 186 (2021), 110105, https://doi.org/10.1016/j.measurement.2021.110105.

[39] Z. Orhan, M. Yilmaz, S. Aydogan, M. Taskin, U. Incekara, Improving light-sensing behavior of Cu/n-Si photodiode with Human Serum Albumin: microelectronic and dielectric characterization, Optik 241 (2021), 167069, https://doi.org/10.1016/j.ijleo.2021.167069.

[40] R. Chandra Neetika, V.K. Malik, Temperature dependent current-voltage characteristics of Pt/MoS2 Schottky junction, MRS Adv 4 (2019) 2127–2134, https://doi.org/10.1557/adv.2019.283.

[41] P. Caprioglio, C.M. Wolff, O.J. Sandberg, A. Armin, B. Rech, S. Albrecht, D. Neher, M. Stolterfoht, On the origin of the ideality factor in perovskite solar cells, Adv. Energy Mater. 10 (2020), 2000502, https://doi.org/10.1002/aenm.202000502.

[42] Ş. Karataş, N. Berk, Performance of the illumination dependent electrical and photodiode characteristic of the Al/(GO:PTCDA)/p-Si structures, Opt. Mater. 126 (2022), 112231, https://doi.org/10.1016/j.optmat.2022.112231.

[43] H. Kaçuş, Ç. Çırak, Ş. Aydoğan, Effect of illumination intensity on the characteristics of Co/Congo Red/p-Si/Al hybrid photodiode, Appl. Phys. Mater. Sci. Process 126 (2020) 1–8, https://doi.org/10.1007/s00339-019-3242-0.

[44] M. Benhaliliba, A rectifying Al/ZnO/pSi/Al heterojunction as a photodiode, Micro Nanostruct. 163 (2022), 107140, https://doi.org/10.1016/j.spmi.2021.107140.

[45] X. Liu, F. Li, M. Xu, J. Qi, Self-powered, high response and fast response speed metal-insulator-semiconductor structured photodetector based on 2D MoS2, RSC Adv. 8 (2018) 28041–28047, https://doi.org/10.1039/c8ra05511d.

[46] H. Norde, A modified forward I-V plot for Schottky diodes with high series resistance, J. Appl. Phys. 50 (1979) 5052–5053, https://doi.org/10.1063/1.325607.
[47] Ş. Aydoğan, Ü. İncekara, A. Türüt, The effects of 12 MeV electron irradiation on the electrical characteristics of the Au/Aniline blue/p-Si/Al device, Microelectron, Reliab 51 (2011) 2216–2222, https://doi.org/10.1016/J.MICROREL.2011.06.002.
[48] M.O. Erdal, A. Kocyigit, M. Yıldırım, Temperature dependent current-voltage characteristics of Al/TiO2/n-Si and Al/Cu:TiO2/n-Si devices, Mater. Sci. Semicond. Process. 103 (2019), 104620, https://doi.org/10.1016/j.mssp.2019.104620.
[49] S.K. Cheung, N.W. Cheung, Extraction of Schottky diode parameters from forward current-voltage characteristics, Appl. Phys. Lett. 49 (1986) 85, https://doi.org/10.1063/1.97359.
[50] D.E. Yıldız, H.H. Gullu, L. Toppare, A. Cirpan, Analysis of temperature-dependent forward and leakage conduction mechanisms in organic thin film heterojunction diode with fluorine-based PCBM blend, J. Mater. Sci. Mater. Electron. 31 (2020) 15233–15242, https://doi.org/10.1007/s10854-020-04088-x.
[51] A. Kocyigit, M. Yılmaz, Ş. Aydoğan, Ü. İncekara, The effect of measurements and layer coating homogeneity of AB on the Al/AB/p-Si devices, J. Alloys Compd. 790 (2019) 388–396, https://doi.org/10.1016/j.jallcom.2019.03.179.
[52] L. Reissig, S. Dalgleish, K. Awaga, A differential photodetector: detecting light modulations using transient photocurrents, AIP Adv. 6 (2016), 15306, https://doi.org/10.1063/1.4939921.
[53] A. Kocyigit, D.E. Yıldız, A.A. Hussaini, D.A. Kose, M. Yıldırım, Cu and Mn centered nicotinamide/nicotinic acid complexes for interlayer of Schottky photodiode, Curr. Appl. Phys. 45 (2023) 53–63, https://doi.org/10.1016/j.cap.2022.11.001.
[54] J. Kublitski, A. Hofacker, B.K. Boroujeni, J. Benduhn, V.C. Nikolis, C. Kaiser, D. Spoltore, H. Kleemann, A. Fischer, F. Ellinger, K. Vandewal, K. Leo, Reverse dark current in organic photodetectors and the major role of traps as source of noise, Nat. Commun. 12 (2021) 1–9, https://doi.org/10.1038/s41467-020-20856-z.
[55] K. Liu, M. Sakurai, M. Aono, ZnO-based ultraviolet photodetectors, Sensors 10 (2010) 8604–8634, https://doi.org/10.3390/s100908604.
[56] W. Xie, F. Cao, L. Wang, X. Ji, High responsivity and EQE of single ZnO:Sb microwire/Ti 3 C 2 T x heterojunction UV photodetector, ACS Appl. Opt. Mater. (2023), https://doi.org/10.1021/acsaom.2c00187.
[57] A. Kumar, S. Mukherjee, H. Sharma, D.K. Rana, A. Kumar, R. Kumar, R.K. Choubey, Fabrication of low-cost and fast-response visible photodetector based on ZnS:Mn/p-Si heterojunction, Mater. Sci. Semicond. Process. 155 (2023), 107226, https://doi.org/10.1016/j.mssp.2022.107226.
[58] A. Kumar, M. Kumar, V. Bhatt, S. Mukherjee, S. Kumar, H. Sharma, M.K. Yadav, S. Tomar, J.H. Yun, R.K. Choubey, Highly responsive and low-cost ultraviolet sensor based on ZnS/p-Si heterojunction grown by chemical bath deposition, Sensors Actuators, A Phys. 331 (2021), 112988, https://doi.org/10.1016/j.sna.2021.112988.
[59] S.J. Chang, B.G. Duan, C.H. Hsiao, S.J. Young, B.C. Wang, T.H. Kao, K.S. Tsai, S. L. Wu, Low-frequency noise characteristics of in-doped ZnO ultraviolet photodetectors, IEEE Photon. Technol. Lett. 25 (2013) 2043–2046, https://doi.org/10.1109/LPT.2013.2280719.
[60] Z.A. Jezeh, B. Efafi, B. Ghafary, The effect of electrode shape on Schottky barrier and electric field distribution of flexible ZnO photodiode, Sci. Rep. 11 (2021) 1–11, https://doi.org/10.1038/s41598-021-95203-3.
[61] L. Agarwal, S. Tripathi, High responsivity ZnO based p-n homojunction UV-photodetector with series Schottky barrier, Semicond. Sci. Technol. 35 (2020), 065001, https://doi.org/10.1088/1361-6641/ab7b0a.
[62] V. Balasubramani, J. Chandrasekaran, V. Manikandan, T.K. Le, R. Marnadu, P. Vivek, Upgraded photosensitivity under the influence of Yb doped on V2O5 thin films as an interfacial layer in MIS type Schottky barrier diode as photodiode application, J. Solid State Chem. 301 (2021), 122289, https://doi.org/10.1016/j.jssc.2021.122289.
[63] S.M. Kumbhar, S.S. Shevate, A.R. Patil, S.K. Shaikh, K.Y. Rajpure, Dip coated TiO2 based metal-semiconductor-metal ultraviolet photodetector for UV A monitoring, Superlattice. Microst. 141 (2020), 106490, https://doi.org/10.1016/j.spmi.2020.106490.
[64] D.B. Patel, K.R. Chauhan, W.H. Park, H.S. Kim, J. Kim, J.H. Yun, Tunable TiO2 films for high-performing transparent Schottky photodetector, Mater. Sci. Semicond. Process. 61 (2017) 45–49, https://doi.org/10.1016/j.mssp.2016.12.036.
[65] S. Agrohiya, V. Kumar, I. Rawal, S. Dahiya, P.K. Goyal, V. Kumar, R. Punia, Fabrication of n-TiO2/p-Si photo-diodes for self-powered fast ultraviolet photodetectors, Silicon 14 (2022) 11891–11901, https://doi.org/10.1007/s12633-022-01913-2.
[66] L. Valdman, V. Mazánek, P. Marvan, M. Serra, R. Arenal, Z. Sofer, Layered ZnIn2S4 single crystals for ultrasensitive and wearable photodetectors, Adv. Opt. Mater. 9 (2021), 2100845, https://doi.org/10.1002/adom.202100845.
[67] A. Kocyigit, A. Akbar Hussaini, M. Yıldırım, D. Ali Kose, D. Esra Yıldız, Schottky type photodiodes with organic Co-complex and Cd-complex interlayers, Appl. Organomet. Chem. (2022). https://doi.org/10.1002/aoc.6879.